npj | climate and atmospheric science

www.nature.com/npjclimatsci

ARTICLE OPEN

Check for updates

Dynamics and characteristics of dry and moist heatwaves over East Asia

Kyung-Ja Ha[1,2]✉, Ye-Won Seo[1,3]✉, Ji-Hye Yeo[1,2], Axel Timmermann[1,3], Eui-Seok Chung[4]✉, Christian L. E. Franzke[1,3], Johnny C. L. Chan[5], Sang-Wook Yeh[6] and Mingfang Ting[7]

The increasing frequency of heatwaves over East Asia (EA) is impacting agriculture, water management, and people's livelihood. However, the effect of humidity on high-temperature events has not yet been fully explored. Using observations and future climate change projections conducted with the latest generation of Earth System models, we examine the mechanisms of dry and moist heatwaves over EA. In the dry heatwave region, anticyclonic circulation has been amplified after the onset of heatwaves under the influence of the convergence of anomalous wave activity flux over northern EA, resulting in surface warming via adiabatic processes. In contrast, the moist heatwaves are triggered by the locally generated anticyclonic anomalies, with the surface warming amplified by cloud and water vapor feedback. Model simulations from phase six of the Coupled Model Intercomparison Project projected display intensification of dry heatwaves and increased moist heatwave days in response to projected increases in greenhouse gas concentrations.

npj Climate and Atmospheric Science (2022)5:49 ; https://doi.org/10.1038/s41612-022-00272-4

INTRODUCTION

Against the backdrop of global warming, heatwaves have become a major meteorological disaster[1]. They have severe impacts on human health[2], agriculture[3], and energy consumption[4]. Exposure to extreme heat is already a significant public health problem that is often related to cardiovascular problems[5] and is a leading cause of weather-related mortality in the United States[6], Asia[7], and Europe[8]. In 2013, China experienced long-lasting and widespread heatwaves that affected more than half a billion people in over nine provinces[9]. In 2018, a record-breaking heatwave occurred on the Korean Peninsula causing heat-related illnesses in 4508 people and 48 deaths[10]. The frequency and duration of heatwave events are increasing globally[11,12]. In the Northern Hemisphere, warm days (defined as the number of days above the 90th percentile of daily mean temperature over the 1961–1990 period) increased by 2.18 days per decade from 1948 to 2006[13]. According to climate model simulations, heatwaves are expected to further intensify in response to increasing concentrations of greenhouse gases[14]. The study of Sun et al.[15] showed that the number of heatwave days in eastern China reached a historical high of 31 days in the summer of 2013, and they suggested that more than 50% of summers in the 2030s will reach daily mean temperatures higher than the maximum temperature in 2013 due to anthropogenic effects. It has recently been documented[16] that global warming has already increased the frequency of extreme high temperature events in China leading to an increasing trend of heat-related mortality.

The World Meteorological Organization distinguishes two types of meteorological heatwaves: dry and moist heatwaves. Dry heatwaves are characterized by stable conditions, clear skies, and a large input of solar radiation, whereas moist heatwaves are often accompanied by very oppressive, humid conditions during the day and night, often with nocturnal cloud cover[17].

Dry summer heatwaves, an example of a "compound extreme", can have severe impacts on agriculture, ecosystems, water supplies, and local economies[18–20]. Zhang et al.[21] reported that the sudden increase in dry and hot extremes over inner East Asia over the last two decades is associated with persistent soil moisture deficits. Zscheischler and Seneviratne[22] found that the frequency of simultaneously occurring hot and dry summers will increase 10-fold during the 21st century as compared to the historical time period (1870–1969). Although recent studies[23] have reported that there is no statistically significant trend in drought risk in the southern and western United States, the risk of co-occurring severe droughts and heatwaves has increased sharply. In addition, over the last few decades, northern China has experienced frequent summer heatwaves that are associated with drought and desertification trends[24–26], and Kong et al.[27] found that heatwave and drought events were more frequent in the North and South of eastern China and less frequent in the central region during 1962–2015.

Globally, the atmosphere is expected to become moister in response to global warming[28,29], however, moisture availability and the moisture-holding capacity of the atmosphere exhibit distinct regional patterns. Some studies have considered the connection between high humidity and heatwaves[30], because of their combined effect on human thermoregulation[31] and loss of labor productivity[32]. In Chicago in 1995 and China in 2003, the magnitude of heatwaves and maximum temperatures were strongly amplified by the effect of humidity[33]. By analyzing climate model simulations under the RCP4.5 and RCP8.5 scenarios for the period 2070–2100 in CMIP5, Kang and Elfahir[34] suggested that the North China Plain will likely experience severe heatwaves with increasing humidity due to irrigation. Ha and Yun[35] further emphasized that surface water vapor acts to trap more heat from the surface at nighttime. Therefore, the combination of high

[1]Center for Climate Physics, Institute for Basic Science, Busan, South Korea. [2]Department of Atmospheric Sciences, Pusan National University, Busan, South Korea. [3]Pusan National University, Busan, South Korea. [4]Korea Polar Research Institute, Incheon, South Korea. [5]School of Energy and Environment, City University of Hong Kong, Hong Kong, China. [6]Department of Marine Science and Convergence Engineering, Hanyang University, Ansan, South Korea. [7]Lamont-Doherty Earth Observatory, Columbia University, Palisades, NY, USA. ✉email: kjha@pusan.ac.kr; ywseo@pusan.ac.kr; echung@kopri.re.kr

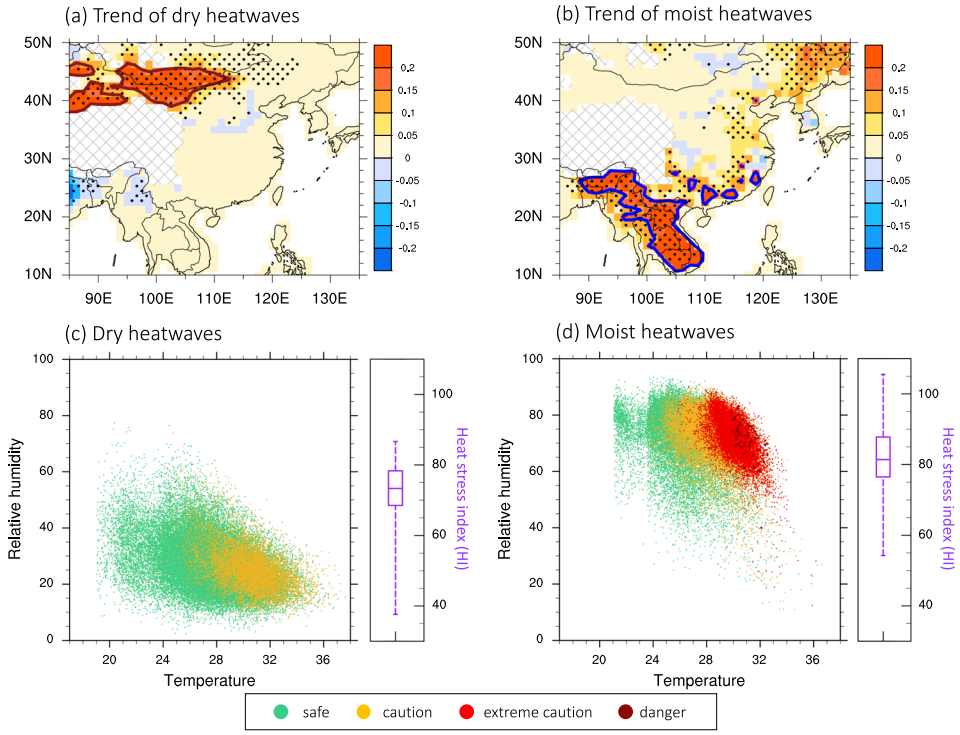

Fig. 1 Linear trends of dry/moist heatwave durations and scatterplot of temperature and relative humidity during heatwave days. **a** Trend of dry heatwaves and **b** trend of moist heatwaves [days year^{-1}]. Heatwaves were defined as periods in which the daily mean temperature was above the 90th percentile for at least 3-days (based on JRA-55 data from 1958 to 2019). The dots indicate the 90% confidence level using *P*-values; hatched lines represent geopotential height above 2000 m; red and blue contours represent areas with trend above 0.15 days year^{-1} during 1958–2019 for **a** dry and **b** moist heatwaves, respectively. Scatterplots of 2 m air temperature and 2 m relative humidity (obtained from JRA-55) during heatwave events over regions where the trends of **c** dry and **d** moist heatwave durations were above 0.15 days year^{-1}, respectively. The green, yellow, red, and dark red colors indicate heat stress categories: safe, caution, extreme caution, and danger, respectively. The purple boxes in **c** and **d** are the ranges of the heat stress index (HI) during dry and moist heatwave days, respectively. The different percentiles depicted in each box are, respectively, the 75th, 50th, and 25th percentile values and the upper and lower lines denote the 90th and 10th percentile values, respectively.

temperature and humidity is a powerful stressor for terrestrial ecosystems and human health.

There are few studies that compare and analyze dry and moist heatwaves. Some previous studies examined the spatial distribution and trends of two types of heatwaves. For instance, Ding and Qian (2011)[36] investigated the geographical patterns and temporal variation of regional dry and wet heatwaves in China. Fu et al. (2021)[37] examined the regional trends of dry and moist heatwaves in different sub-regions of China, and An and Zou (2021)[38] identified different circulation types associated with dry and moist heatwave in North China using the Self-Organizing Map. Despite these previous studies, they did not focus on the mechanisms to understand the occurrence of heatwaves. Therefore, further investigations are needed to better understand the underlying mechanisms of the two types of heatwaves. Our study focuses on the regional trends and features of dry and moist heatwaves over East Asia (EA) from 1958 to 2019 and their underlying physical causes. Our aim is to elucidate the dynamical and thermodynamical mechanisms involved in different types of heatwave events. We then determine the heatwave trends using the Japanese 55-year reanalysis dataset (JRA-55)[39] data and future human-induced heatwave trends using multi-model projections from the Coupled Model Intercomparison Project phase 6 (CMIP6).

RESULTS

Distinguishing dry and moist heatwaves

In order to characterize the dynamics of heatwaves over EA, we analyze the total duration (days year^{-1}) of heatwaves during the warm season (from May to October) (see Methods). To determine the causes of heatwave events with humidity conditions, we define dry and moist heatwaves as heatwaves having relative humidity below 33% and above 66%, respectively. Regional trends in the duration of heatwaves over 1958–2019 showed that dry heatwaves increased and were dominant over northwestern EA adjacent to the main desert regions, whereas the occurrence frequency of moist heatwaves increased, especially, over southern EA and closer to the maritime moisture sources (Fig. 1a, b). The duration of heatwaves defined only by temperature without consideration of the humidity condition increased over both of these areas (Supplementary Fig. 1). The relationship between temperature and relative humidity was investigated over the region where dry and moist heatwave trends were above 0.15 days year^{-1} for all heatwave events from 1958 to 2019. Hereafter, these regions are referred to as dry and moist heatwave regions, respectively. In the dry (moist) heatwave regions, dry (moist) heatwaves accounted for 68% (79%) of all heatwave events. There is an uneven distribution of water sources between the South and North of EA: water is abundant in the South and less so in the North. Therefore, regional differences exist in terms of relative humidity.

To characterize the simultaneous effects of moisture and temperature on human health, we calculated a heat stress index[40,41] (HI) for EA (see Supplementary Methods). Over the past 62 years dry heatwaves in EA (Fig. 1c) have reached the category of the heat stress "caution" level, whereas numerous moist heatwaves occurred in the southern part of EA for which the HI index reached levels of "extreme caution" and even "danger"

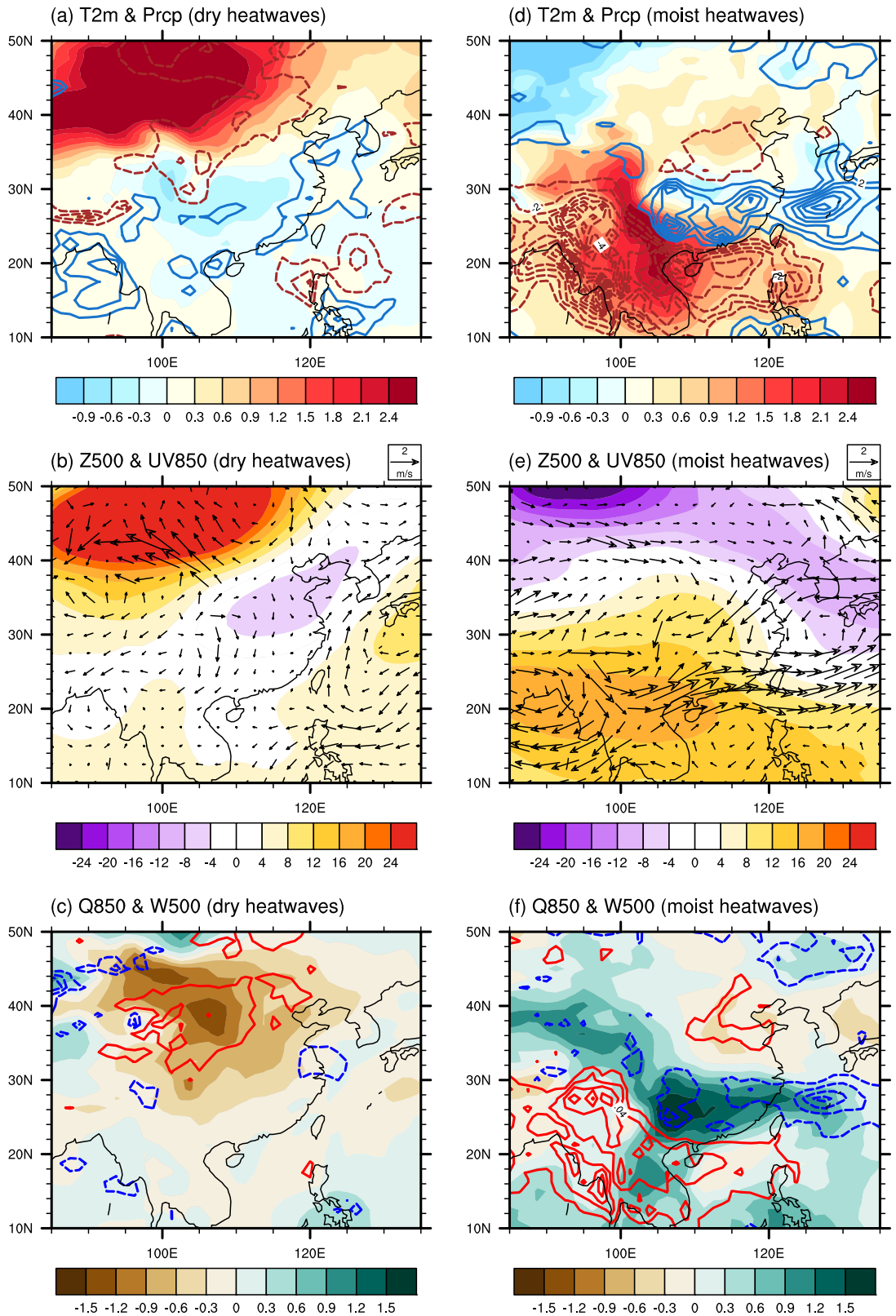

Fig. 2 Anomaly composites for heatwave days over dry/moist heatwave regions. Anomaly composites relative to long-term daily mean (climatology) of **a**, **d** 2 m air temperature (shading) [°C] and precipitation (contours) [mm day^{-1}], **b**, **e** geopotential height at 500-hPa (shading) [m] and wind at 850 hPa (vectors) [m s^{-1}], and **c**, **f** specific humidity at 850 hPa (shading) [g kg^{-1}] and omega at 500 hPa (contours) [Pa s^{-1}] for **a**–**c** dry heatwave days and **d**–**f** moist heatwave days. Dry and moist heatwave days were determined as days on which the heatwaves occurred simultaneously in more than 40% of the regions where the trend was more than 0.15 days year^{-1} for dry and moist heatwaves, respectively.

(Fig. 1d). This further illustrates the necessity to analyze dry and humid heatwaves separately.

Mechanisms for the two types of heatwaves over East Asia

To determine the underlying mechanisms of dry and moist heatwaves, we calculated the anomalous composites of atmospheric variables during heatwave days over the dry and moist heatwave regions (Fig. 2; Supplementary Fig. 2), where anomalies for each variable are defined relative to the long-term daily means values over the period of 1958–2019.

Dry and moist heatwave days were determined as days during which the heatwaves occurred simultaneously in more than 40% of the regions with trend above 0.15 days year^{-1} for dry and moist heatwaves, respectively. In the dry and moist heatwave regions, warm anomalies and less precipitation are prevalent, which is consistent with anomalous anti-cyclonic flow and a sinking motion (Fig. 2; Supplementary Fig. 2). The descending motion provided sunny weather, which enabled solar radiation to reach the land surface unimpeded. These features, which usually prevail during heatwave activity, are evident over dry heatwave regions. The moist heatwaves are accompanied by additional moisture to southern EA through the moist advection from the adjacent ocean (Supplementary Fig. 3b).

Previous studies have shown that heatwaves are affected by synoptic-scale systems such as blocking high or Rossby waves[10,42,43]. For instance, studies of heatwaves over China have found that the regions where heatwaves occurred vary depending on the synoptic-scale atmospheric circulation structures[25,44]. Therefore, we identified the origin of the anticyclonic circulation on the synoptic-scale influencing the formation of heatwaves through the corresponding spatiotemporal evolution of atmospheric circulation and the wave activity flux (WAF) (see "Methods"; Fig. 3).

For dry heatwaves, the WAF is mainly directed eastward in the middle and high latitudes in accordance with the wave train from Europe (Fig. 3a–e). From three days prior to the heatwave's occurrence or earlier, prominent positive anomalies of geopotential height at 700 hPa develop over Central Asia. The WAF analysis suggests that the wave propagation originating from Western Europe acts to amplify anticyclonic anomalies over northern EA and thus contributes to the formation of dry heatwaves (Fig. 3a–e). Through anomalous WAF convergence and divergence can be analyzed the growth or decay characteristics of the ridge[45]. It means that the anomalous WAF convergence in the upstream develops the ridge. The anomalous WAF convergence in the northern EA amplified the ridge in the dry heatwave region (Supplementary Fig. 4a–e). Moreover, the mid-latitude wave train is related to 500 hPa geopotential height composite anomalies during all dry heatwave days (Supplementary Fig. 5a). Our analysis reveals that the anticyclonic anomalies induced by the atmospheric wave trains are the main cause of dry heatwaves. This wave structure is still maintained up to 3 days after the onset and it is bound up with the development of heatwaves (Fig. 3d, e; Supplementary Fig. 4d, e).

Anticyclonic anomalies are located over the moist heatwave region from a day before the onset (Fig. 3g, h). This anomalous high is induced by convergence of the anomalous WAF onto Bangladesh (Fig. 3h–j; Supplementary Fig. 4h–j) and provides favorable conditions for surface warming through increasing downward solar radiation. This result has led to heatwaves over the moist heatwave region. Moreover, the composite anomalies of the SST and the 500 hPa geopotential height show that moist heatwaves are related to warm SST anomalies over the warm pool region and the Indian Ocean (Supplementary Fig. 5b).

To further elucidate the contribution from dynamic and thermodynamic effects to the development of dry and moist heatwaves, we calculated the composite of the energy budget at the surface and the temperature budget at 975 hPa during the five days before and the onset day of the heatwave (see "Methods"; Fig. 4; Supplementary Fig. 6). In the dry heatwave regions, a greater amount of solar radiation than 5 days before the onset can reach the surface associated with anticyclonic anomalies, leading to an increase in the surface air temperature. As the surface dries, latent heat flux decreases despite fewer changes in evapotranspiration (Fig. 4a; Supplementary Figs. 6a and 7a, c). The latent heat not used for evaporation contributes to heating the surface. The sensible heat flux does not change much between 5 days before and onset days. However, as the median value of sensible heat flux is about 3.4 times larger than that of latent heat flux on onset day, it is expected to play a role in warming the surface (Supplementary Fig. 6a). A further temperature budget analysis at 975 hPa showed that adiabatic heating, which likely is caused by downward motion, plays a role in warming the dry heatwave region (Figs. 2e, 4c; Supplementary Fig. 6c). The local temperature tendency is 0.82 °C day^{-1} higher (median value) during the onset day than 5-days before.

In the moist heatwave region, the enhanced downward solar radiation and surface-to-atmosphere latent heat flux are mainly due to anomalous subsidence anomaly (Figs. 2f, 4b; Supplementary Figs. 6b, 2f). The latent heat flux due to the increase in evapotranspiration increases on the onset day compared to 5-days before (Fig. 4b; Supplementary Figs. 6b, 7b, d). However, the diabatic heating associated with anomalous latent heat flux increase is largely compensated by the sum of the advection and adiabatic terms induced by strong northwesterly anomalies and anomalous sinking motion (Figs. 2e, f, 4d). Therefore, the local temperature tendency is increased by about 0.02 °C day^{-1} (median value) on the onset day compared to 5-days before (Fig. 4d). The distinctive characteristics and underlying physical processes for the different regions indicate that we have to account for both humidity and temperature to properly assess the impact of heatwaves for instance on agriculture and human health.

Feedback attribution on dry and moist heatwaves in EA

We further investigated partial changes in surface land temperature between the strong and normal dry/moist heatwave years resulting from several individual feedback processes through the climate feedback-response analysis method (CFRAM) analysis (Eq. (6) in the "Methods"). Total temperature changes related to the dry heatwave represent warm anomalies over the dry heatwave regions (Fig. 5a), and the latent heat flux and surface dynamics are major drivers of the heatwave-related temperature pattern (Fig. 5g, h). The sensible and latent heat fluxes play opposite roles in surface temperature change in the dry heatwaves. The partial temperature changes caused by the latent heat flux are due to the decrease in the surface-to-atmosphere latent heat flux. It is associated with decreasing evaporative cooling or transpiration of water at the land surface, thus it contributed to the warming of the surface by reducing heat release from the surface to the atmosphere[46]. Surface dynamics processes provided positive temperature anomalies over dry heatwave regions. It is mainly caused by changes in soil heat diffusion or heat storage. In contrast, the water vapor, sensible heat flux, and atmospheric dynamics processes give a negative contribution to the warming of the total temperature change (Fig. 5c, f, i).

Meanwhile, cloud feedback and water vapor feedback are primary drivers of significant warming anomalies over the moist heatwave region (Fig. 5l, n). Since the moist heatwave regions are affected by summer monsoon, these have many clouds in summer. However, the decreased cloud amount and reduced precipitation occurred due to subsidence motions during the

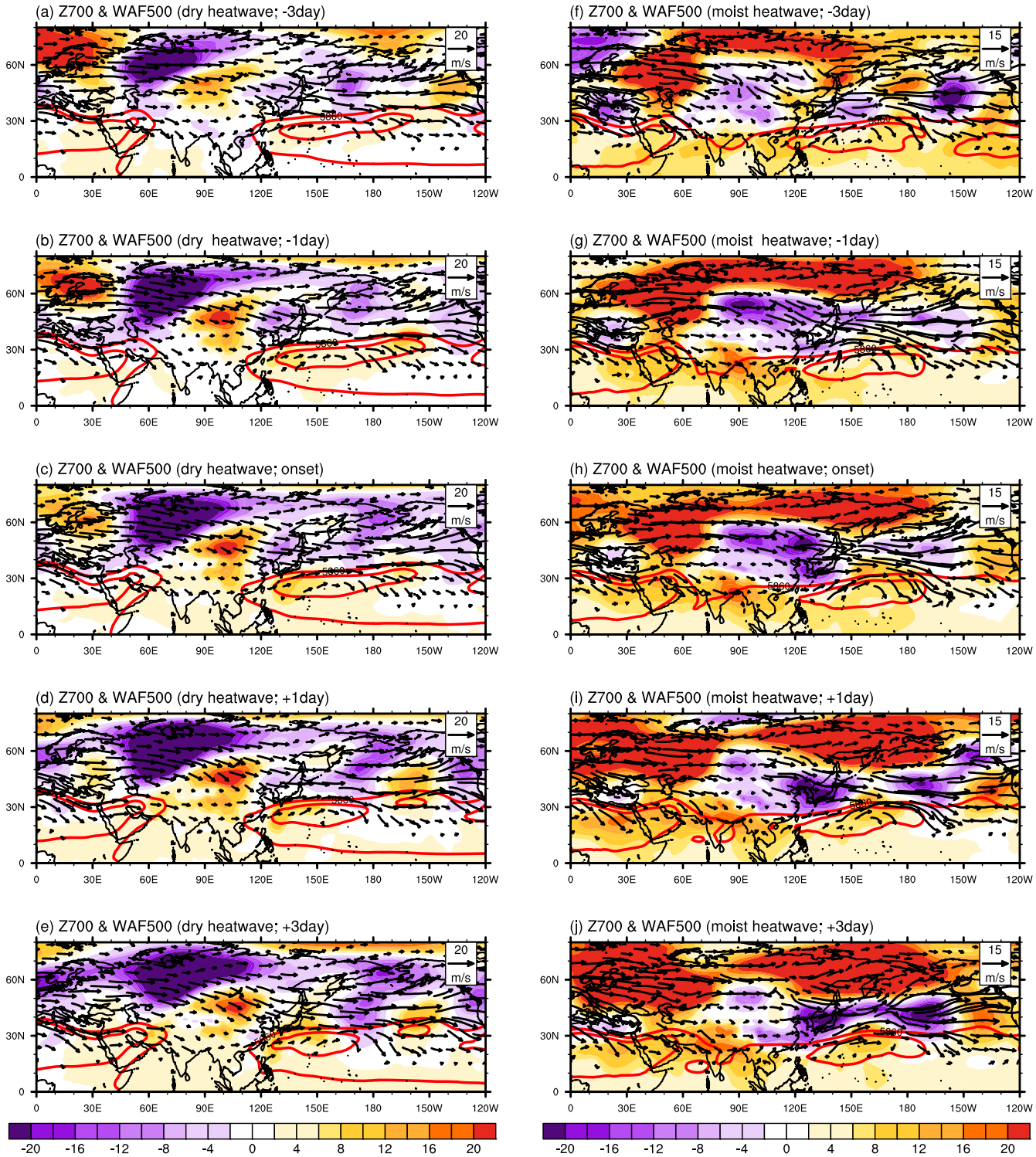

Fig. 3 Wave propagation from 3 days prior to onset up to 3 days after onset of heatwaves. Composite maps of geopotential height anomalies at 700 hPa (shading), geopotential height at 500 hPa (red contours), and wave activity flux (WAF) at 500 hPa (vectors) before and after the occurrence of **a**–**e** dry heatwaves and **f**–**j** moist heatwaves. To computed the WAF, the definition proposed by Takaya and Nakamura (2001, JAS) was used. The normal state of the geopotential height is represented by the daily mean for the period 1958–2019.

heatwave events. Hence, less cloud cover related to enhanced anticyclonic anomalies makes positive contributions to the surface warming over moist heatwave regions by increasing the insolation. The positive water vapor feedback associated with increased surface-to-atmosphere latent heat flux contributes to the warming of the surface, reflecting the moistening of air.

Projected dry and moist heatwaves in EA

We estimated the multi-model ensemble (MME) changes in the linear trend of dry and moist heatwaves from the CMIP6 historical simulation for the period 1958–2014 and Shared Socioeconomic Pathway 2–4.5 (SSP2–4.5) scenario for the period from 2015 to 2100 (Fig. 6a–d; Supplementary Table 1). We calculate the 90th

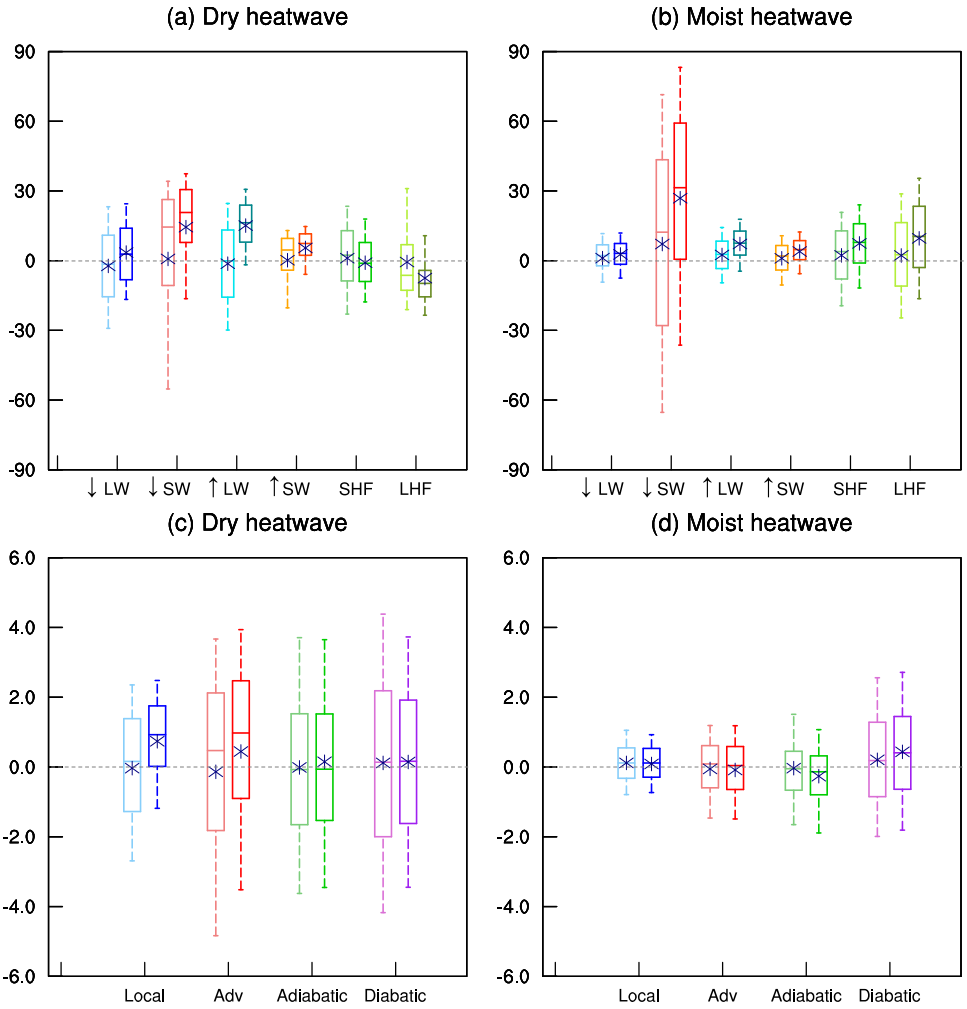

Fig. 4 Anomalies of surface energy budget and temperature budget at 975 hPa for dry/moist heatwave days. Amomalies of surface energy budget (left axis) including downward longwave (↓LW) and shortwave radiation flux (↓SW) [W m^{-2}], upward longwave (↑LW) and shortwave radiation flux (↑SW) [W m^{-2}], surface sensible (SHF) and latent heat flux (LHF) [W m^{-2}] associated with **a** dry heatwaves and **b** moist heatwaves during the 5-day period before the onset (left boxes) and on onset-day (right boxes). Note that positive values of latent and sensible heat fluxes denote heat flux tranfer from the surface to the atmosphere. Temperature budget terms at 975 hPa during the 5-days before onset (left boxes) and on onset-day (right boxes) associated with **c** dry heatwaves and **d** moist heatwaves [°C day^{-1}]. * denotes the mean value, and the different percentiles depicted in each box are, respectively, the 75th, 50th, and 25th percentile values. The upper and lower lines denote the 90th percentile and the 10th percentile value, respectively.

percentile threshold of daily mean temperature from historical climate simulation, and the dry and moist heatwaves are identified using this threshold (Supplementary Fig. 8). Most of the CMIP6 models exhibit dry heatwave trend patterns that are very similar to those of the observations, but some models show large discrepancies in the moist heatwave trends (Supplementary Figs. 9, 10). The regions exhibiting a positive trend are projected to expand over much of EA in response to increasing concentrations of greenhouse gases (Fig. 6a–d). The results of the SSP5–8.5 scenario are similar to the low emission scenario, but their amplitudes are higher (Supplementary Fig. 11a, b). In particular, dry and moist heatwave trends are projected to increase by up to 0.3 days (0.41 days and 0.83 days) and 0.54 days (1.53 days and 2.19 days) per year, respectively, for historical simulation (SSP2–4.5 and SSP5–8.5) (Fig. 6a–d; Supplementary Fig. 11a, b). At the end of the 21st century for SSP2–4.5 (SSP5–8.5), dry heatwaves are projected to occur for 44.2 days (70.6 days) and moist heatwaves for 73 days (122.1 days) during the warm season (Fig. 6e, f; Supplementary Fig. 11c, d). The number of heatwave days over the moist heatwave region more than doubles compared to the dry heatwave region. We show that heat extremes will become more frequent in the future for high emission scenarios, and 38.4 and 66.4% of warm seasons will be hotter than the present in the dry and moist heatwave regions under the SSP5–8.5 scenario, respectively. The trend patterns of dry and moist heatwaves for the SSP1–1.9 scenario are similar to the SSP2–4.5 and SSP5–8.5 (Fig. 6c, d; Supplementary Figs. 11a, b and 12a, b). The number of both dry and moist heatwave days increases in the middle of the 21st century, then drops back by 2100 due to the large-scale deployment of negative emissions technologies (Supplementary Fig. 12c, d).

To quantify changes in dry and moist heatwaves in response to anthropogenic warming, we examined the timing of heatwaves from March to October of individual years within the 1958–2100 period based on historical climate simulations (Fig. 6g, h). It indicates the heatwave activity including the occurrence, duration, starting date of the first episode, and amplitudes.

The historical simulations showed that dry heatwaves occurred more frequently than moist heatwaves (Fig. 6g, h). In the dry heatwave region, the severe heatwave (>3.0 °C) will gradually increase after 2047 (Fig. 6g). About 20.1% of the warm season in 2100 is projected to experience extreme heatwaves due to

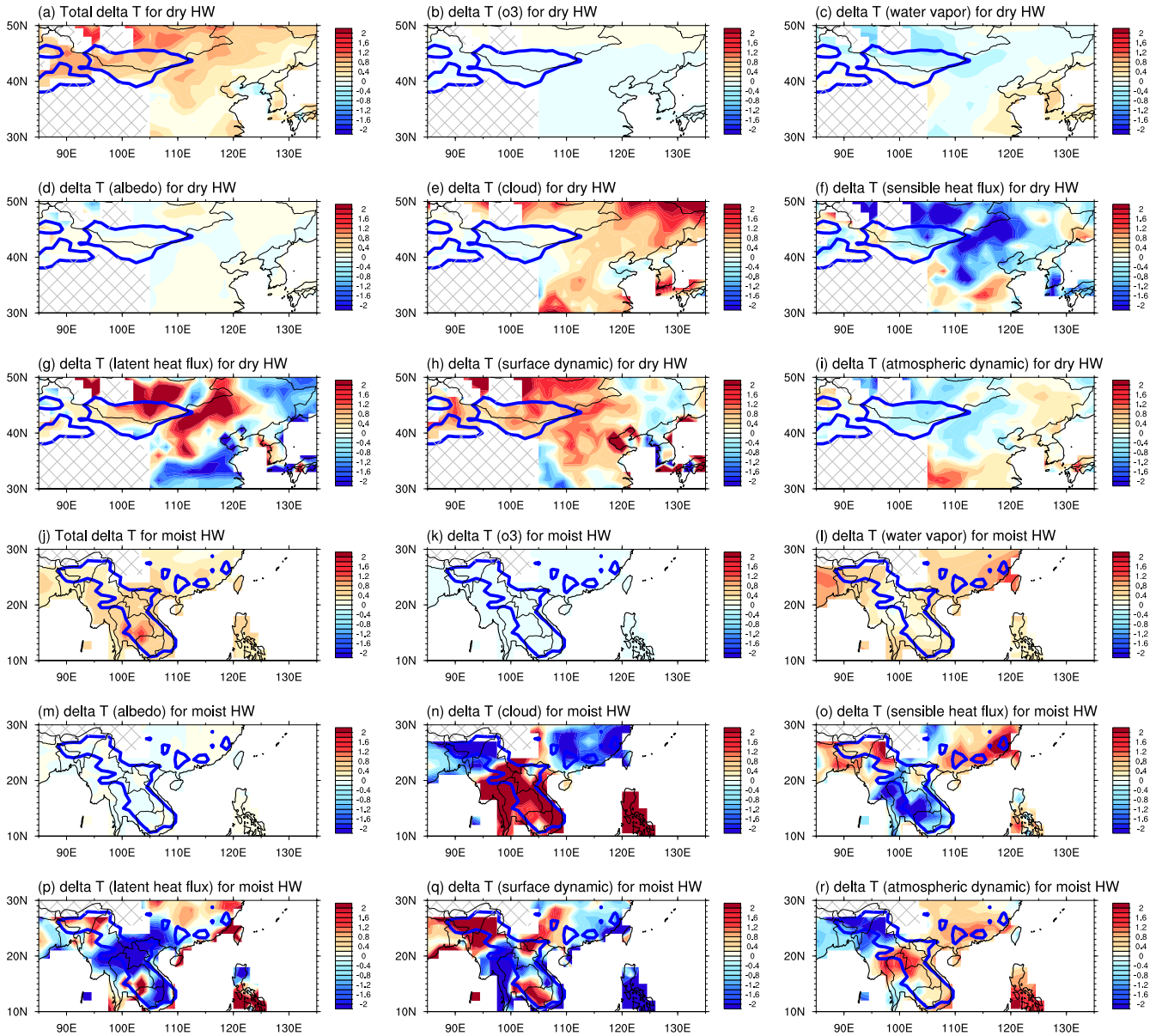

Fig. 5 Partial temperature changes due to feedback attributions in dry/moist heatwaves. a Total temperature anomalies [K] and CFRAM-derived partial temperature changes due to **b** ozone feedback, **c** water vapor feedback, **d** surface albedo feedback, **e** cloud feedback, **f** sensible heat flux change, **g** latent heat flux change, **h** surface dynamics, and **i** atmospheric dynamics in composite dry heatwave summer. **j**–**r** Same as (**a**–**i**) but for moist heatwaves. The red and blue contours represent areas with trend above 0.15 days year^{-1} based on JRA-55 data during 1958–2019 for **a**–**i** dry and **j**–**r** moist heatwaves, respectively. The hatched areas indicate above 2000 m in geopotential height.

anthropogenic effects under SSP2–4.5 scenario. However, our findings suggest that future moist heatwave events become more frequent and will last longer. In particular, the total days of moist heatwaves are expected to increase. In the moist heatwave region, 82% of the warm season in 2100 will experience heatwave conditions (Fig. 6h). They will start in March and persist until late September (or even October; Fig. 6h; Supplementary Fig. 11f), especially enhanced heatwave (>1.5 °C) will frequently occur in early summer after 2039 under SSP2–4.5 scenario. The intensity of both dry and moist heatwaves will be enhanced. The amplitude of dry heatwaves will increase up to 4.9 K (8.2 K) for SSP2–4.5 (SSP5–8.5) compared to the 90th percentile of daily mean temperature for the historical scenario (Fig. 6g; Supplementary Figs. 8 and 11e). The result that the intensity of the hottest days over extratropical regions and the frequency of extremely hot days over the tropics are projected to increase is consistent with the results of Almazroui et al.[47]. Despite projected reductions in greenhouse gas emissions, the intensity and duration of heatwaves will become amplified over dry and moist heatwave regions for SSP1–1.9 (Supplementary Fig. 12e, f). In summary, the MME results show that dry heatwaves will become more frequent with enhanced amplitudes (Fig. 6g), and moist heatwaves will occur for prolonged periods with an earlier start and a later end of heatwave seasons (Fig. 6h).

DISCUSSION

Studying the large-scale meteorological patterns associated with heatwave events provides a framework for understanding their underlying causal mechanisms. This study is novel for two reasons: first, it separately investigates the synoptic settings and tele-connection patterns associated with heatwaves to better

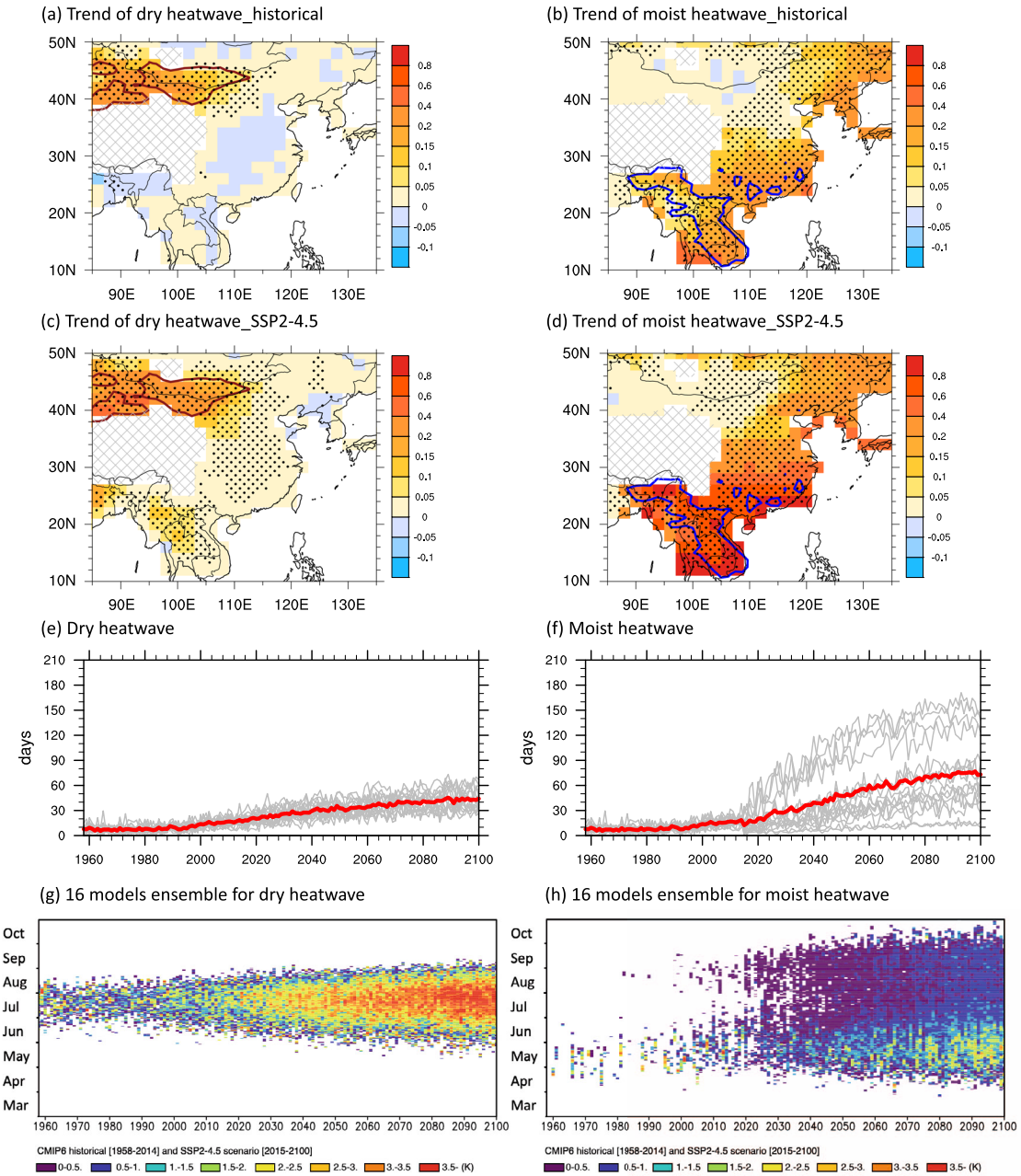

Fig. 6 Heatwaves over dry/moist heatwave regions using JRA-55, CMIP6 historical, and SSP2-4.5 scenario. a Trend of dry heatwave days per year and **b** moist heatwaves during the period from 1958 to 2014 based on the multi-model mean. Heatwaves were defined as days on which the 90th percentile of daily mean temperature was reached for at least 3-days, based on the historical run simulation of each model from 1958 to 2014. The dots indicate the 90% confidence level using the *P*-value. The red and blue contours in **a** and **b** represent areas with trend above 0.15 days year^{-1} based on JRA-55 data during 1958–2019 for dry and moist heatwaves, respectively. The hatched areas indicate above 2000 m in geopotential height. **c** and **d** are the same as **a** and **b** but, respectively, for SSP2–4.5. Time series of heatwave durations over **e** dry and **f** moist heatwave regions (brown contour in (**a**) and blue contour in (**b**)). The gray lines denote the results of each model and the red lines indicate the result of the multi-model ensemble mean. The timing of (**g**) dry and (**h**) moist heatwaves from March to October during 1958–2014 based on the historical climate simulation and during 2015–2100 based on the SSP2–4.5 scenario in the multi-model mean of CMIP6. Data are shown for regions with trend above 0.15 days year^{-1} for dry and moist heatwaves, respectively. The color scale shows the difference between the daily mean temperature and the 90th temperature percentile. For the future projection, we used the 90th temperature percentiles based on the period from 1958 to 2014 from the historical run simulation of each model.

understand the underlying mechanisms; and second, it attempts to determine heatwave onset mechanisms by linking dry/moist heatwave trends to the surface energy budget and thermodynamic processes.

Several previous studies have found that hot and humid events are more detrimental to human health than hot and dry events[16,48]. On the other hand, hot and dry events have a substantial effect on water resources and agriculture[49]. Heatwave projection studies[34,50,51] have emphasized the relationship between anthropogenic effects and increasing heatwaves, but regional aspects have not previously been explored. For example, Kang and Eltahir[34] and Im et al.[50] showed that irrigation is affecting climate change, and this may increase the risk from heatwaves in eastern China. This current study emphasizes the

fact that certain regions in China are likely to experience deadly heatwaves with humidity conditions that exceed thresholds stipulated in outdoor working conditions. Heat stress influenced by combined temperature and humidity effects will increasingly disrupt economic activity. Although the world is committed to limiting the rise in global mean temperature to 1.5 °C by the end of the century, according to the Paris Agreement, it is envisaged that the accumulated financial losses associated with heat stress will reach US$2.4 trillion by 2030[51]. Both dry and moist heatwaves are projected to increase over East Asia under three different SSP scenarios, although the magnitude is different between the scenarios. Increases in heatwaves are also expected even in the low emission SSP1–1.9 scenario, in which the greenhouse gas emissions meet the Paris Agreement's 1.5 °C goal. This similarity suggests the robustness of projected increases in both dry and moist heatwaves over East Asia, and implies that these increases may be unavoidable in the future. In addition, more efforts are needed to keep the temperature below 1.5 °C to not experience the increasing heatwave days, and these efforts may reduce our exposure to heat stress we will face in the future[52,53]. We expect that these implications provide insights into the attributes of the dry and moist heatwaves.

It is also important to highlight the substantial differences between future changes in the two types of heatwaves. The selected 16 CMIP6 model simulations reveal that heatwave events will become more frequent and they will last longer. In addition, the amplitude of dry heatwaves will be enhanced and moist heatwaves will begin to occur earlier in the year and their durations over southern EA will increase. Our results suggest that in-depth research involving observations and climate model simulations is required to further elucidate the mechanisms involved in moist and dry heatwaves. Such information can then be further translated into the associated impacts on human health, agricultural, and related ecosystem stress. Studies are also required in other areas of the world focusing on how dry and moist heatwaves will respond to anthropogenically generated warming. In summary, these results show that characterizing heatwaves in different regions and determining their underlying physical processes is essential for providing more accurate information on combined effects of humidity and temperature. It would help to enable the development of agricultural and water resource adaptation strategies.

METHODS

Definitions of dry and moist heatwaves

In this study, a heatwave event was defined as one in which temperatures exceeded the 90th percentile of the daily mean temperature during the warm season (May to October) for at least three consecutive days. To characterize the heatwaves, we analyzed the total duration (days year^{-1}) of heatwaves that caused unhealthy thermal exposure and human suffering during the total warm season. The total number of heatwaves represented the sum of heatwave days during the considered period: 11408 days for 62 years from 1958 to 2019 (62 years × 184 days in each year). We also defined dry and moist heatwaves by the presence of relative humidity below 33% or above 66%, respectively, during the same days. Hereafter, we refer to regions where the dry and moist heatwave trends are greater than 0.15 days year^{-1} as dry and moist heatwave regions, respectively. Dry and moist heatwave days were selected as a day with a heatwave occurring over more than 40% of the dry and moist heatwave region, respectively.

The analysis domain of this study is the EA region between 85°E–135°E and 10°N–50°N. Daily mean 2 m temperatures and 2 m relative humidity were used to identify heatwaves occurring over EA. We also excluded high terrain regions (>2 km) to eliminate low-temperature heatwaves.

Wave activity flux (WAF)

To track the propagation of wave flow, we analyzed the WAF as defined by Takaya and Nakamura[45]. The WAF vectors represent the movement of the stationary wave and the anomalous WAF convergence and divergence zone is expected to amplify or decay the ridge in geopotential height. It is useful to track the time evolution and flow of the ridge associated with the development of each heatwave. The WAF defined by Takaya and Nakamura is as follows:

$$\mathrm{W}=\frac{p\cos\phi}{2|U|}\begin{pmatrix}\frac{U}{a^2\cos^2\phi}\left[\left(\frac{\partial\psi'}{\partial\lambda}\right)^2-\psi'\frac{\partial^2\psi'}{\partial\lambda^2}\right]+\frac{V}{a^2\cos\phi}\left[\frac{\partial\psi'}{\partial\lambda}\frac{\partial\psi'}{\partial\phi}-\psi'\frac{\partial^2\psi'}{\partial\lambda\partial\phi}\right]\\ \frac{U}{a^2\cos^2\phi}\left[\frac{\partial\psi'}{\partial\lambda}\frac{\partial\psi'}{\partial\phi}-\psi'\frac{\partial^2\psi'}{\partial\lambda\partial\phi}\right]+\frac{V}{a^2}\left[\left(\frac{\partial\psi'}{\partial\phi}\right)^2-\psi'\frac{\partial^2\psi'}{\partial\phi^2}\right]\\ \frac{f_0^2}{N^2}\left\{\frac{U}{a\cos\phi}\left[\frac{\partial\psi'}{\partial\lambda}\frac{\partial\psi'}{\partial z}-\psi'\frac{\partial^2\psi'}{\partial\lambda\partial z}\right]+\frac{V}{a}\left[\frac{\partial\psi'}{\partial\phi}\frac{\partial\psi'}{\partial z}-\psi'\frac{\partial^2\psi'}{\partial\phi\partial z}\right]\right\}\end{pmatrix} \quad (1)$$

where p, a, f_0, N, ϕ, and λ are the pressure normalized by 1000 hPa, the Earth's radius, the Coriolis parameter at 45°N, the Brunt–Väisälä frequency, the latitude, and the longitude, respectively. The geostrophic stream-function (ψ) is defined as Φ/f, where Φ is the geopotential and f ($=2\Omega\sin\phi$) is the Coriolis parameter with the Earth's rotation rate as Ω.

Climate feedback-response analysis method (CFRAM)

The climate feedback-response analysis method (CFRAM) was developed by Lu and Cai[54] based on the energy balance in both the atmosphere and the surface within a column at a given horizontal location consisting of M atmospheric layers and a surface layer. In this study, we considered the difference in energy balance between two equilibrium states, such as strong and normal dry/moist heatwave years. The two equilibrium states such as strong and normal dry/moist heatwave years were selected based on normalized time series of heatwaves over dry and moist heatwave regions (Supplementary Fig. 13). The strong years are those when the normalized value is greater than 1.5 standard deviations, and normal years were chosen by excluding the strong years. The energy balance equation can be written as:

$$\Delta\frac{\partial\mathbf{E}}{\partial t}=\Delta\mathbf{S}-\Delta\mathbf{R}+\Delta\mathbf{Q}^{\mathrm{non-radiative}}, \quad (2)$$

where $\Delta\frac{\partial\mathbf{E}}{\partial t}$ is the change in energy storage, $\mathbf{S}$ is the convergence of the shortwave radiation flux, $\mathbf{R}$ is the divergence of the longwave radiation flux, and $\mathbf{Q}^{\mathrm{non-radiative}}$ is the vertical profile of the energy flux convergence due to nonradiative dynamic processes. The right hand sides of Eq. (2) can be linearized and the terms can be separated into partial differences due to individual radiative and non-radiative processes as follows:

$$\Delta\mathbf{S}\approx\Delta\mathbf{S}^{(w)}+\Delta\mathbf{S}^{(c)}+\Delta\mathbf{S}^{(a)}+\Delta\mathbf{S}^{(O_3)}, \quad (3)$$

$$\Delta\mathbf{R}\approx\Delta\mathbf{R}^{(w)}+\Delta\mathbf{R}^{(c)}+\Delta\mathbf{R}^{(O_3)}+\frac{\partial\mathbf{R}}{\partial\mathbf{T}}\Delta\mathbf{T}, \quad (4)$$

$$\Delta\mathbf{Q}^{\mathrm{non-radiative}}=\Delta\mathbf{Q}^{(\mathrm{SH})}+\Delta\mathbf{Q}^{(\mathrm{LH})}+\Delta\mathbf{Q}^{(\mathrm{atmos\_dyn})}+\Delta\mathbf{Q}^{(\mathrm{sfc\_dyn})}, \quad (5)$$

where w, c, a, O_3, SH, LH, atmos_dyn, and sfc_dyn represent water vapor, cloud, surface albedo, ozone, sensible heat flux, latent heat flux, atmospheric dynamics, and surface dynamics, respectively. $\frac{\partial\mathbf{R}}{\partial\mathbf{T}}$ is the Planck feedback matrix in which the jth column represents the vertical profile of changes in longwave radiative energy flux resulting from 1-K warming in the jth layer[55]. Substituting Eqs. (3)–(5) into Eq. (2) we obtain

$$\begin{aligned}\Delta\mathbf{T}=\left(\tfrac{\partial\mathbf{R}}{\partial\mathbf{T}}\right)^{-1}\Big\{&\Delta(\mathbf{S}-\mathbf{R})^{(w)}+\Delta(\mathbf{S}-\mathbf{R})^{(c)}+\Delta(\mathbf{S}-\mathbf{R})^{(O_3)}\\&+\Delta\mathbf{S}^{(a)}+\Delta\mathbf{Q}^{(SH)}+\Delta\mathbf{Q}^{(LH)}+\Delta\mathbf{Q}^{(atmos\_dyn)}+\Delta\mathbf{Q}^{(sfc\_dyn)}\Big\}.\end{aligned} \quad (6)$$

It is noted that the local temperature differences between two climate states can be decomposed into partial temperature from individual feedback processes. The radiative energy differences and the Plank feedback matrix are performed using the Fu-Liou radiative transfer model[56]. More detailed information about the CFRAM can be found in refs. [46,54,57].

The CMIP6 models

To analyze the characteristics of model-projected heatwaves, we used data from 16 CMIP6 climate models from historical simulations for the period 1958–2014 and from the SSP2–4.5 and SSP5–8.5 scenarios for the period 2015–2100: CanESM5, CESM2-WACCM, CNRM-CM6–1, CNRM-ESM2-1, EC-Earth3, EC-Earth3-Veg, FGOALS-g3, GFDL-CM4, GFDL-ESM4, INM-CM4–8, INM-CM5-0, IPSL-CM6A-LR, MIROC6, MPI-ESM1-2-HR, MRI-ESM2-0, and UKESM1-0-LL. Details of the 16 CMIP6 models are provided in Supplementary Table 1. All models were interpolated to a 2.0° × 2.0° spatial resolution prior to analysis. It is of note that only the first ensemble member ("r1i1p1f1") was used for each model, but other ensemble

members were considered if the first ensemble member was unavailable (e.g., CNRM-CM6, CNRM-ESM2-1, and UKESM1-0-LL ("r1i1p1f2"). We also analyzed the characteristics of projected heatwaves under a low emission scenario (i.e., SSP1-1.9), in which the rise in global-mean temperature is limited to 1.5 °C by 2100, using simulation output from eight of the 16 models: CanESM5, EC-Earth3-Veg, FGOALS-g3, GFDL-ESM4, IPSL-CM6A-LR, MIROC6, MRI-ESM2-0, UKESM1-0-LL.

DATA AVAILABILITY

The datasets analyzed in this study are daily 2 m air temperature and 2 m relative humidity, geopotential height, zonal and meridional winds, vertical velocity, precipitation rate, upward and downward shortwave radiation flux, upward and downward longwave radiation flux, net surface latent and sensible heat flux, and top cloud cover from JRA-55 (https://jra.kishou.go.jp/JRA-55/index_en.html)[39]. In addition, the National Oceanic and Atmospheric Administration (NOAA) High-resolution Blended Analysis of Daily Sea surface temperature (SST) and Ice data (OISST) were used from 1982 to 2019[58] (https://www.esrl.noaa.gov/psd/data/gridded/data.noaa.oisst.v2.highres.html). We used ERA-Interim reanalysis datasets[59] for calculating the CFRAM (http://apps.ecmwf.int/datasets/). Input variables for CFRAM analysis are atmospheric/surface temperature, specific humidity, ozone mixing ratio, cloud liquid/ice water content, cloud fraction, sensible/latent heat flux, surface pressure, and surface albedo. CMIP6 data are from https://esgf-node.llnl.gov/search/cmip6/.

CODE AVAILABILITY

The NCL and fortran codes used to run the analysis can be obtained upon request to the corresponding authors.

Received: 9 August 2021; Accepted: 27 May 2022;
Published online: 21 June 2022

REFERENCES

1. Trenberth, K. E. & Josey S. A. *Climate Change 2007: The Physical Science Basis. Contribution of Working Group I to the Fourth Assessment Report of the Intergovernmental Panel on Climate Change* (eds Solomon, S. et al.) (Cambridge University Press, 2007).
2. Pantavou, K., Theoharatos, G., Mavrakis, A. & Santamouris, M. Evaluating thermal comfort conditions and health responses during an extremely hot summer in Athens. *Build. Environ.* **46**, 339–344 (2011).
3. Asseng, S., Foster, I. & Turner, N. C. The impact of temperature variability on wheat yields. *Glob. Chang. Biol.* **17**, 997–1012 (2011).
4. Hadley, S. W., Erickson, D. J., Hernandez, J. L., Broniak, C. T. & Blasing, T. J. Responses of energy use to climate change: A climate modeling study. *Geophys. Res. Lett.* **33**, L17703 (2006).
5. Marsh, T. J. The 1995 UK drought—a signal of climatic instability? *Proc. Inst. Civ. Eng. Munic. Eng.* **118**, 189–195 (1996).
6. Howe, P. D., Marlon, J. R., Wang, X. & Leiserowitz, A. Public perceptions of the health risks of extreme heat across US states, counties, and neighborhoods. *Proc. Natl Acad. Sci. USA* **116**, 6743–6748 (2019).
7. Tan, J. et al. The urban heat island and its impact on heat waves and human health in Shanghai. *Int. J. Biometeorol.* **1850**, 75–84 (2010).
8. Garcia-Herrera, R., Díaz, J., Trigo, R. M., Luterbacher, J. & Fischer, E. M. A review of the european summer heat wave of 2003. *Crit. Rev. Environ. Sci. Technol.* **40**, 267–306 (2010).
9. Hou, W. et al. Climatic characteristics over China in 2013. *Meteorol. Mon.* **40**, 491–501 (2014).
10. Ha, K. J. et al. What caused the extraordinarily hot 2018 summer in Korea? *J. Meteorol. Soc. Jpn.* **98**, 153–167 (2020).
11. Meehl, G. A. & Tebaldi, C. More intense, more frequent, and longer lasting heat waves in the 21st century. *Science* **305**, 994–997 (2004).
12. Rahmstorf, S. & Coumou, D. Increase of extreme events in a warming world. *Proc. Natl Acad. Sci. USA* **108**, 17905–17909 (2011).
13. Fang, X., Wang, A., Fong, S., Lin, W. & Liu, J. Changes of reanalysis-derived Northern Hemisphere summer warm extreme indices during 1948-2006 and links with climate variability. *Glob. Planet. Change* **63**, 67–78 (2008).
14. Saeed, F., Almazroui, M., Islam, N. & Khan, M. S. Intensification of future heat waves in Pakistan: A study using CORDEX regional climate models ensemble. *Nat. Hazards* **87**, 1635–1647 (2017).
15. Sun, Y. et al. Rapid increase in the risk of extreme summer heat in Eastern China. *Nat. Clim. Chang.* **4**, 1082–1085 (2014).
16. Wang, Y. et al. Tens of thousands additional deaths annually in cities of China between 1.5 °C and 2.0 °C warming. *Nat. Commun.* **10**, 1–7 (2019).
17. McGregor, G. R., Bessemoulin, P., Ebi, K. & Menne, B. Heat waves and health: Guidance on warning system development. Geneva, Switzerland, World Meteorological Organization and World Health Organization (2015).
18. Fischer, E. M. & Schär, C. Consistent geographical patterns of changes in high-impact European heatwaves. *Nat. Geosci.* **3**, 398–403 (2010).
19. Perkins, S. E., Alexander, L. V. & Nairn, J. R. Increasing frequency, intensity and duration of observed global heatwaves and warm spells. *Geophys. Res. Lett.* **39**, 1–5 (2012).
20. Trenberth, K. E. et al. Global warming and changes in drought. *Nat. Clim. Chang.* **4**, 17–22 (2014).
21. Zhang, P. et al. Abrupt shift to hotter and drier climate over inner East Asia beyond the tipping point. *Science* **370**, 1095–1099 (2020).
22. Zscheischler, J. & Seneviratne, S. I. Dependence of drivers affects risks associated with compound events. *Sci. Adv.* **3**, 1–11 (2017).
23. Mazdiyasni, O. & AghaKouchak, A. Substantial increase in concurrent droughts and heatwaves in the United States. *Proc. Natl Acad. Sci. USA* **112**, 11484–11489 (2015).
24. Zhai, P. et al. Changes of climate extremes in China. *Clim. Change* **42**, 203–218 (1999).
25. Wang, W., Zhou, W., Li, X., Wang, X. & Wang, D. Synoptic-scale characteristics and atmospheric controls of summer heat waves in China. *Clim. Dyn.* **46**, 2923–2941 (2016).
26. Ding, Y. et al. Detection, causes and projection of climate change over China: An overview of recent progress. *Adv. Atmos. Sci.* **24**, 954–971 (2007).
27. Kong, Q., Guerreiro, S. B., Blenkinsop, S., Li, X. F. & Fowler, H. J. Increases in summertime concurrent drought and heatwave in Eastern China. *Weather Clim. Extrem.* **28**, 100242 (2020).
28. IPCC. *Climate Change 2007: Synthesis Report*. *Climate Change 2007: Synthesis Report* https://doi.org/10.1256/004316502320517344 (2007)
29. Held, H. I. M. & Soden, J. B. Robust reponses of the hydrological cycle to gloal warming. *J. Clim.* **19**, 5686–5699 (2006).
30. Sherwood, S. C. How important is humidity in heat stress? *J. Geophys. Res. Atmos.* **123**, 11808–11810 (2018).
31. Schär, C. Climate extremes: The worst heat waves to come. *Nat. Clim. Chang.* **6**, 128–129 (2016).
32. Dunne, J. P., Stouffer, R. J. & John, J. G. Reductions in labour capacity from heat stress under climate warming. *Nat. Clim. Chang.* **3**, 563–566 (2013).
33. Russo, S., Sillmann, J. & Sterl, A. Humid heat waves at different warming levels. *Sci. Rep.* **7**, 7477 (2017).
34. Kang, S. & Eltahir, E. A. B. North China plain threatened by deadly heatwaves due to climate change and irrigation. *Nat. Commun.* **9**, 2894 (2018).
35. Ha, K. J. & Yun, K. S. Climate change effects on tropical night days in Seoul, Korea. *Theor. Appl. Climatol.* **109**, 191–203 (2012).
36. Ding, T. & Qian, W. Geographical patterns and temporal variations of regional dry and wet heatwave events in China during 1960–2008. *Adv. Atmos. Sci.* **28**, 322–337 (2011).
37. Xu, F., Chan, T. O. & Luo, M. Different changes in dry and humid heat waves over China. *Int. J. Climatol.* **41**, 1369–1382 (2021).
38. An, N. & Zuo, Z. Investigating the influence of synoptic circulation patterns on regional dry and moist heat waves in North China. *Clim. Dyn.* **57**, 1227–1240 (2021).
39. Kobayashi, C. & Iwasaki, T. Brewer-Dobson circulation diagnosed from JRA-55. *J. Geophys. Res. Atmos.* **121**, 1493–1510 (2016).
40. Sun, Q., Miao, C., Hanel, M., Borthwick, A. G. L. & Duan, Q. Global heat stress on health, wildfires, and agricultural crops under different levels of climate warming. *Environ. Int.* **128**, 125–136 (2019).
41. Coffel, E. D., Horton, R. M. & De Sherbinin, A. Temperature and humidity based projections of a rapid rise in global heat stress exposure during the 21st century. *Environ. Res. Lett.* **13**, 014001 (2018).
42. Brunner, L., Hegerl, G. C. & Steiner, A. K. Connecting atmospheric blocking to European temperature extremes in spring. *J. Clim.* **30**, 585–594 (2017).
43. Röthlisbergera, M., Frossard, L., Bosart, L. F., Keyser, D. & Martius, O. Recurrent synoptic-scale Rossby wave patterns and their effect on the persistence of cold and hot spells. *J. Clim.* **32**, 3207–3226 (2019).
44. Chen, R. & Lu, R. Comparisons of the circulation anomalies associated with extreme heat in different regions of eastern China. *J. Clim.* **28**, 5830–5844 (2015).
45. Takaya, K. & Nakamura, H. A formulation of a phase-independent wave-activity flux for stationary and migratory quasigeostrophic eddies on a zonally varying basic flow. *J. Atmos. Sci.* https://doi.org/10.1175/1520-0469(2001)0582.0.CO;2 (2002).
46. Seo, Y.-W., Ha, K.-J. & Park, T.-W. Feedback attribution to dry heatwaves over East Asia. *Environ. Res. Lett.* **16**, 064003 (2021).

47. Almazroui, M. et al. Projected changes in climate extremes using CMIP6 simulations over SREX regions. *Earth Syst. Environ.* **5**, 481–497 (2021).
48. McInnes, J. A. et al. Association between high ambient temperature and acute work-related injury: A case-crossover analysis using workers' compensation claims data. *Scand. J. Work. Environ. Heal.* **43**, 86–94 (2017).
49. Piao, S. et al. The impacts of climate change on water resources and agriculture in China. *Nature* **467**, 43–51 (2010).
50. Im, E., Pal, J. S. & Eltahir, E. A. B. Deadly heat waves projected in the densely populated agricultural regions of South Asia. *Sci. Adv.* **3**, e1603322 (2017).
51. Kjellstrom, T., Maître, N., Saget, C., Otto, M. & Karimova, T. Working on a warmer planet: The impact of Heat Stress on Labour Productivity and Decent Work. Geneva, Switzerland, International Labour Office (2019).
52. Saeed, F., Schleussner, C. F. & Ashfaq, M. Deadly heat stress to become commonplace across South Asia already at 1.5 °C of global warming. *Geophys. Res. Lett.* **48**, 1–11 (2021).
53. Saeed, F., Schleussner, C. F. & Almazroui, M. From Paris to Makkah: Heat stress risks for Muslim pilgrims at 1.5 °C and 2 °C. *Environ. Res. Lett.* **16**, 024037 (2021).
54. Lu, J. & Cai, M. A new framework for isolating individual feedback processes in coupled general circulation climate models. Part I: Formulation. *Clim. Dyn.* **32**, 873–885 (2009).
55. Wetherald, R. T. & Manabe, S. Cloud feedback processes in a general circulation model. *J. Atmos. Sci.* **45**, 1397–1415 (1988).
56. Fu, Q. & Liou, K. N. On the correlated k-distribution method for radiative transfer in nonhomgeneous atmospheres. *J. Atmos. Sci.* **49**, 2139–2156 (1992).
57. Cai, M. & Lu, J. A new framework for isolating individual feedback processes in coupled general circulation climate models. Part II: Method demonstrations and comparisons. *Clim. Dyn.* **32**, 887–900 (2009).
58. Reynolds, R. W. et al. Daily high-resolution-blended analyses for sea surface temperature. *J. Clim.* **20**, 5473–5496 (2007).
59. Dee, D. P. et al. The ERA-Interim reanalysis: Configuration and performance of the data assimilation system. *Q. J. R. Meteorol. Soc.* **137**, 553–597 (2011).

ACKNOWLEDGEMENTS

We are grateful for the assistance provided by the following with respect to important input on our early manuscript: Fei-Fei Jin, Jianping Li, and Kyong-Hwan Seo. This study was supported by the Institute for Basic Science (project code IBS-R028-D1) and the National Foundation of Korea (NRF) grant funded by the Korea government (MSIT) (Grant No. 2020R1A2C2006860).

AUTHOR CONTRIBUTIONS

K.-J.H. and A.T. designed and conceived the research, Y.-W.S. and J.-H.Y. contributed to the graphics and analyzed the model outputs, K.-J.H., Y.-W.S., and J.-H.Y. wrote the early draft and K.-J.H., A.T., E.-S.C., C.L.E.F., J.C.L.C., S.-W.Y., and M.T. contributed to writing the manuscript.

COMPETING INTERESTS

The authors declare no competing interests.

ADDITIONAL INFORMATION

Supplementary information The online version contains supplementary material available at https://doi.org/10.1038/s41612-022-00272-4.

Correspondence and requests for materials should be addressed to Kyung-Ja Ha, Ye-Won Seo or Eui-Seok Chung.

Reprints and permission information is available at http://www.nature.com/reprints

Publisher's note Springer Nature remains neutral with regard to jurisdictional claims in published maps and institutional affiliations.